Published in final edited form as:

Biochemistry. 2022 March 01; 61(5): 311–318. doi:10.1021/acs.biochem.1c00759.

Structural Insights into Molecular Recognition by Human Chemokine CCL19

Eric M. Lewandowski[1], **Kyle G. Kroeck**[1], **Lian M.C. Jacobs**[1], **Tyler G. Fenske**[2], **Robin N. Witt**[3], **Alyssa M. Hintz**[3], **Elizabeth R. Ramsden**[3], **Xiujun Zhang**[1], **Francis Peterson**[2], **Brian F. Volkman**[2,*], **Christopher T. Veldkamp**[3,*], **Yu Chen**[1,*]

[1]Department of Molecular Medicine, University of South Florida Morsani College of Medicine, 12901 Bruce B. Downs Blvd., Tampa, Florida 33612, United States

[2]Department of Biochemistry and Program in Chemical Biology, Medical College of Wisconsin, Milwaukee, Wisconsin 53226, United States

[3]Department of Chemistry, University of Wisconsin Whitewater, Whitewater, Wisconsin 53190, United States

Abstract

The human chemokines CCL19 and CCL21 bind to the G-protein coupled receptor (GPCR) CCR7 and play an important role in the trafficking of immune cells, as well as cancer metastasis. Conserved binding sites for sulfotyrosine residues on the receptor contribute significantly to the chemokine/GPCR interaction and have been shown to provide promising targets for new drug-discovery efforts to disrupt the chemokine/GPCR interaction, and consequently tumor metastasis. Here, we report the first X-ray crystal structure of a truncated CCL19 (residues 7–70) at 2.50 Å resolution, revealing molecular details crucial for protein-protein interactions. Although the overall structure is similar to the previously determined NMR model, there are important variations, particularly near the N-terminus and the so-called 30's and 40's loops. Computational analysis using the FTMap server indicates the potential importance of these areas in ligand binding, and the differences in binding hot spots compared to CCL21. NMR titration experiments using a CCR7-derived peptide (residues 5–11, TDDYIGD) further demonstrates potential receptor recognition sites, such as those near the C-terminus and 40's loop, that consist of both positively charged and hydrophobic residues which may be important for receptor binding. Taken together, the X-ray, NMR, and computational analysis herein provides insights into the overall structure and molecular features of CCL19 and enables investigation into this chemokine's function and inhibitor development.

Graphical Abstract

*Corresponding authors: Brian F. Volkman, bvolkman@mcw.edu, Christopher T. Veldkamp, veldkamc@uww.edu, Yu Chen, ychen1@usf.edu.

Conflict of Interest

B.F.V and F.C.P. have ownership interests in Protein Foundry, LLC and XLock Biosciences, LLC.

Accession Codes

The structure coordinates have been deposited in the Protein Data Bank with access code 7STA. CCL19 has UniProt ID Q99731.

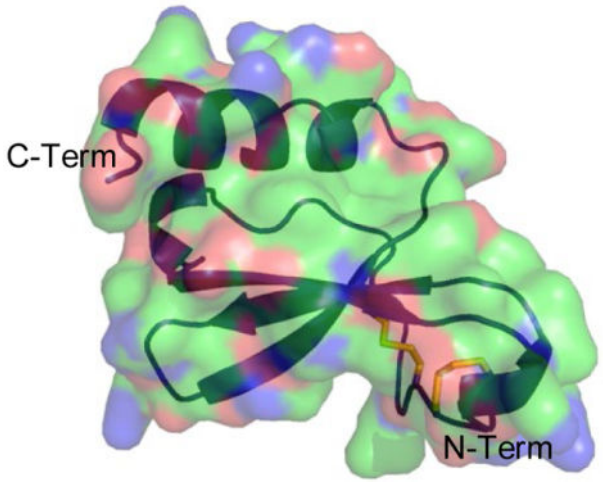

Introduction

Chemokines are a group of small (8–17 kDa) signaling proteins that direct cell migration involved with immune response through binding to, and activation of, their associated G-protein coupled receptors (GPCRs).[1] There are four chemokine subfamilies, with grouping dependent on the number of amino acids present between conserved N-terminal cysteine residues (CXC, CC, CX3C, and XC).[2] Accordingly, the associated chemokine receptors are classified based on which chemokine they bind to (CXCR, CCR, CX3CR, XCR).[2] The chemokine receptor CCR7 is activated by two CC-chemokines, CCL19 and CCL21, and activation of CCR7 plays a significant role in the metastasis of some cancers; particularly, lymphomas and leukemias.[1, 3–5] CCL19 differs from CCL21 in that it lacks an elongated 32 residue C-terminal tail containing a third disulfide bond; in contrast to the two conserved disulfide bonds typically found in other chemokines.[6] This long C-terminal tail not only makes CCL21 larger than CCL19, but it results in the two chemokines inducing differential effects in the CCR7 signaling pathway.[1, 3, 7, 8]

Activation of CCR7 by CCL19 appears to play two main roles in the manifestation of disease states; first, by facilitating metastasis of certain forms of T-cell leukemia,[9, 10] and second, through the development of a latent infection when activation is followed by HIV-1 infiltration of resting T-cells.[11, 12] Development of this latent HIV-1 infection is one of the main reasons that many effective antiretroviral drugs are unable to completely abolish the virus.[11–13] The role that CCL19 plays in both cancer metastasis and the development of latent HIV-1 infection makes it a prime target for therapeutic development.

Chemokines form protein-protein interactions with their respective receptors, and this interaction follows a general process of receptor activation.[14] First, the flexible N-terminal domain of the chemokine receptor recognizes and binds to the chemokine, and subsequently, the N-terminus of the chemokine binds to the chemokine receptor, ultimately resulting in activation of the receptor and the ensuing downstream cellular effects.[14, 15] A critical component of the interactions between chemokines and their receptors is sulfonation of the tyrosine residues located in the receptor N-terminal domain, as these sulfotyrosines impart a

large amount of the affinity the receptor has for its chemokine ligand.[16, 17] The significance of this sulfotyrosine affinity, and the presence of a sulfotyrosine-binding pocket, appears to be conserved across a large variety of chemokines.[1, 18, 19] These sulfotyrosine-binding pockets make intriguing candidates for new drug-discovery efforts and present a better opportunity than the generally difficult to target protein-protein binding interface.[20, 21] Herein, we present the first X-ray crystal structure of CCL19, together with computational and NMR analysis of its ligand binding hot spots. The results provide important insights into the unique structural features of CCL19 and future inhibitor design against this chemokine.

Materials and Methods

Purification.

The truncated CCL19 sequence (UniProt ID Q99731, residues 7–70) was inserted into a pQE30 vector (Qiagen) along with a SUMO tag (His_6-SMT3) and transformed into BL21/DE3 competent *E. coli* cells. Cells were cultured in 50 mL LB media and incubated overnight. 10 mL of culture was diluted into 1 L of fresh LB media containing 25 μg/mL kanamycin and 50 μg/mL ampicillin. Cells were incubated at 37 °C until reaching an OD_{600} of 1.0 and were then induced with 500 μM IPTG and incubated for an additional 4 h. Cells were then centrifuged at 5,000 × g for 10 min., and the pellet resuspended in 20 mL of 20 mM Tris pH 8.0, 300 mM NaCl, 20 mM imidazole, 0.1% β-mercaptoethanol, and a Pierce Protease Inhibitor tablet (Thermo Scientific). The resuspended cells were then lysed by sonication and centrifuged at 40,000 × g for 40 min. Due to CCL19 being expressed in inclusion bodies, the protein was resuspended in 20 mL of denaturing buffer (20 mM Tris pH 8.0, 6 M Guanidine HCl, 300 mM NaCl, 10 mM imidazole) and incubated in a 37 °C water bath for 1 h., with occasional shaking. The sample was then centrifuged at 40,000 × g for 40 min. and the supernatant collected and filtered.

The sample was then loaded onto a HisTrap affinity column at 1 mL/min and eluted in a single step using Buffer A (100 mM Sodium Acetate pH 4.5, 6 M Guanidine HCl, 300 mM NaCl). The eluted sample was diluted dropwise in 200 mL refolding buffer (100 mM Tris pH 8.0, 10 mM reduced cysteine, 0.5 mM oxidized cysteine (cystine)) and allowed to refold overnight at 4 °C. The SUMO tag was then cleaved off using 2.4 mg of ULP1 and overnight incubation at 30 °C. The cleaved sample was filtered and concentrated, exchanged into Buffer B (20 mM Tris pH 8.0, 300 mM NaCl, 40 mM imidazole), and run through a HisTrap column again at 1 mL/min to remove the cleaved SUMO tag. Eluted sample was collected and concentrated, and then loaded onto a HiLoad 16/60 SuperDex 75 column using Buffer C (20 mM Tris pH 8.0, 150 mM NaCl). Purified CCL19 was concentrated to 13.3 mg/mL, flash frozen, and stored at −80 °C.

Crystallization.

Purified CCL19 (13.3 mg/mL) was screened against the MPD and $AmSO_4$ suites (Qiagen), the JCSG + and PACT screens (Jena Bioscience), and the Berkeley and Top 96 screens (Rigaku) through use of the Crystal Phoenix Liquid Dispensing robot (Art Robbins Instruments). Drops were dispensed in a sitting drop tray in a 1:1 ratio (CCL19:screen), and then incubated at 20 °C in a Rock Imager 1000 hotel (Formulatrix). Crystals appeared after

seven days in a well containing 20% PEG 3350 and 0.2 M sodium nitrate. The condition was scaled up and then optimized by changing the final pH of the crystallization buffer to pH 5.5. Additionally, a drop ratio of 2 μL protein: 2 μL crystallization buffer was used to produce the largest crystals. Crystals were then transferred to a cryo-protectant solution (20% PEG 3350, 0.2 M sodium nitrate, 30% glycerol), harvested, and flash frozen in liquid nitrogen.

X-ray Data Collection, Processing, and Refinement.

Diffraction data was collected using the 19-BM beamline of the Structural Biology Center (SBC) at the Advanced Photon Source (APS), Argonne, Illinois. Data were processed using iMOSFLM[22] and Scala from the CCP4 suite.[23] The CCP4 suite,[23] Coot,[24] and the PDB REDO server (pdb-redo.eu)[25] were used to complete the model building and refinement. The PyMOL Molecular Graphics System (Version 2.4, Schrödinger, LLC) was used to generate all images.

FTMap Analysis.

FTMap analysis was carried out using the FTMap Computational Solvent Mapping Server (ftmap.bu.edu).[26] The server docked a total of 16 different small organic molecules (acetaldehyde; acetamide; acetone; acetonitrile; benzaldehyde; benzene; cyclohexane; dimethyl ether; ethane; ethanol; isobutanol; isopropanol; methylamine; N,N-dimethylformamide; phenol; urea) to the surface of the protein. The PyMOL Molecular Graphics System (Version 2.4, Schrödinger, LLC) was used to visually inspect the results and generate all images.

NMR Analysis.

Recombinant human [U-^{15}N] CCL19 was expressed and purified as previously described.[1, 27] Reverse phase-HPLC purified CCR7 4–9 (VTDDYI-NH2) or CCR7 5–11 (TDDYIGD-NH2) was purchased from a commercial peptide synthesis vendor. Heteronuclear single quantum coherence (HSQC) spectra of 50 μM [U-^{15}N] CCL19 with 0, 25, 50, 75, 100, 200, 300, 800, 1000, 1600, and 2273 μM of either CCR7 4–9 or CCR7 5–11 were collected in the NMR facility at the Medical College of Wisconsin on a Bruker Avance 600 MHz spectrometer equipped with a 1H/13C/15N Cryoprobe® at 25 °C in NMR buffer (25 mM deuterated MES at pH 5.6 with 10% D_2O and 0.02% NaN_3). Changes in CCL19 backbone amide 1H ($\Delta\delta_H$) and 15N ($\Delta\delta_N$) chemical shifts in parts per million (ppm) were combined and computed using the following formula, $[5(\Delta\delta_H)^2 + (\Delta\delta_N)^2]^{1/2}$. Dissociation constants (K_d) were determined using dose dependent changes in chemical shift perturbations and nonlinear fitting to an equation that considers ligand depletion, as previously described.[1]

Results and Discussion

X-ray crystal structure of CCL19

In order to gain a better structural understanding of CCL19 for use in structure-based drug design, we set out to determine the X-ray crystal structure. Initial crystallization trials with the full-length CCL19 did not produce any viable crystallization hits. In order to help

stabilize the protein, we engineered several truncations of the flexible N and C-terminal tails. CCL19 7–70 was crystallized in the $P2_1$ space group (PDB ID: 7STA) and the structure was determined to 2.50 Å resolution (Table 1, Fig. 1). There are four copies of the protein in the asymmetric unit and the R_{Work} and R_{Free} are 23% and 26%, respectively (Table 1). When superimposed, there is good overall similarity amongst the four copies, with the average B-factor for each monomer between 53–60 $Å^2$ (A – 53.61, B – 59.11, C – 54.08, D– 58.60) (Fig. 1). Additionally, all copies exhibit the canonical chemokine fold consisting of a flexible N-terminus and N-loop, an anti-parallel three-stranded β-sheet, a C-terminal α-helix, and a short flexible C-terminus.[1] However, Ser69 and Ala70 of the C-terminal tail, and Asp7 on the N-terminal, were unable to be modeled into the density for chains B and D. Additionally, there is significant variation among the backbone conformation for the Leu10-Glu14 stretch of residues, with chains B and D, and chains A and C adopting similar poses. A significant variation comes at Leu10, with there being three different conformations for the side chain among chains A-D, likely due to the very weak density at this position, thus indicating its flexibility. The two conserved cysteine residues (residues 8 and 9) of the CC motif form disulfide bonds with Cys34 and Cys50 and are readily apparent in the density. The four copies all share extremely similar conformations for the 30's loop (Lys31-Pro37) and 40's loop (Thr43-Gly46), which are turns found in chemokines that connect the β-sheets (30's loop – β1- β2 turn; 40's loop β2- β3 turn).

In comparison to the previously determined NMR structure of CCL19 (PDB ID: 2MP1), the newly obtained crystal structure is similar overall. However, one of the most noticeable differences is a shift in the position of the 30's loop between the two structures. In the crystal structure, the 30's loop is bent significantly downwards and into a position that is not observed in any of the 20 poses of the CCL19 NMR ensemble (Fig. 2). The conformational change between the NMR and crystal structure correlates with the different conformations of the N-terminus, which is in close contact with the 30's loop. The two conserved disulfide bonds near the N-terminus, involving residues 8 and 9 respectively, adopt different conformations in the crystal structure compared to the NMR ensemble. In the NMR structure, the large amount of flexibility demonstrated by the N-terminal tail was also reflected in the variability of the conformation of the conserved cysteines in all 20 poses. In comparison, in the crystal structure these disulfide bonds adopted the same conformation in all four copies in the asymmetric unit, even though the protein backbone following the disulfide bond in the N-terminus exhibited variations in their configurations. Notably, the conformation of the 40's loop remains relatively the same between all chains of the crystal structure and the NMR ensemble, with only minor differences between the conformations of the side chains (the flexible Arg45 in particular). The overall similarity of the crystal structure to the NMR structure is expected. In examining the NMR ensemble, apart from the flexible N and C-terminal regions, the conformation of the structure among the 20 poses was quite conserved. As truncating the flexible regions in the crystal structure did not disrupt the core of the protein, it is not surprising that the truncated CCL19 would adopt the same chemokine fold as seen in the NMR ensemble.

Ligand binding hot spots revealed by FTMap analysis

In a previous study,[28] we used FTMap analysis[26] to probe the surface of the X-ray crystal structure of CCL21 (PDB ID: 5EKI) for potential small molecule binding hot spots. The FTMap server docks 16 small organic probes (see **Methods** for complete list of probes) to the surface of the protein structure, and areas where these probes are found to cluster can indicate a potential binding hot spot that can be targeted for future drug design. Due to the similarity of CCL21 to CCL19, we compared the FTMap results from the CCL21 X-ray crystal structure to the results from our CCL19 X-ray crystal structure to determine if there was any overlap in potential hot spots between the two structures (Fig. 3). The initial comparison of the two results shows that potential binding hot spots between the structures is varied, with one main region of overlap being in an area sandwiched between the N-terminal and the end of the 40's loop. This area contains the cluster with the highest number of probes for CCL21 (Fig. 3B, CL01 – 31 probes) and the third highest cluster for CCL19 (Fig. 3A, CL03 – 16 probes). However, in the CCL21 results, there are four clusters located in this area near the N-terminal loop (Fig 3B, CL01, 04, 05, 06) for a total of 58 probes, while in the CCL19 structure there are only two clusters in the general area (Fig 3A, CL03, 04) for a total of 29 probes. It appears a downwards shift of the N-terminal loop in the CCL19 structure prevents many of the probes from binding in this area. One of the most obvious differences can been seen when looking at the location of the largest cluster of probes in CCL19 (Fig. 3A, CL01 – 20 probes). Although this area near the beginning of the α-helix contains a hot spot with the highest number of probes in CCL19, there are no probes present in this area of the CCL21 structure, despite a very similar fold in that area for both structures. The structural basis for this difference can be seen when viewing the amino acid side chains. In the CCL21 structure, Lys29 protrudes upwards into this area, and appears to block any probes from binding, while this area is open in the CCL19 structure, thus allowing an ample number of probes to bind.

NMR analysis of receptor-derived peptide binding by CCL19

As a part of a chemokine's activation of a chemokine receptor, binding to the receptor's N-terminus is important.[19, 29–37] Numerous studies have used protein NMR to investigate the interaction of chemokines with peptides constituting the chemokine receptor N-terminus.[19, 32–37] Previously, we reported on the interaction of both CCL19 and CCL21 with the N-terminus of the CCR7 receptor as analyzed by protein NMR techniques.[1, 37, 38] Fuchs *et al.* also used microscale thermophoresis (MST) and nano differential scanning fluorimetry (nanoDSF) to analyze the binding of fragments of the CCR7 N-terminus and found some, like CCR7 1–10 (QDEVTDDYIG-NH_2) and CCR7 4–9 (VTDDYI-NH_2), bound with much greater affinity to CCL19 (K_d ~ 800 and 300 nM, respectively) than the full length CCR7 N-terminus (K_d > 1 μM).[39] To determine if CCR7 4–9 occupied any of the CCL19 hotspots identified by FTMap, we monitored the interaction with [U-^{15}N] CCL19 in a 2D NMR titration experiment. The resulting ^{15}N-^{1}H HSQC spectra are overlaid in Figure 4A where it is apparent that most CCL19 signals are unaffected at all concentrations of CCR7 4–9 peptide. A plot of combined amide ^{1}H/^{15}N chemical shift perturbations at the highest concentration of CCR7 4–9 peptide shows that only three residues exhibit shifts > 0.2 ppm. Attempts to estimate the binding affinity from nonlinear fitting of dose dependent

chemical shift perturbations for CCL19 Y27, R45, and R47 were unsuccessful, suggesting that binding of the CCR7 4–9 peptide is very weak and probably non-specific. We observed nothing in the NMR titration, consistent with the sub-micromolar binding affinity reported by Fuchs et al.

We previously used protein NMR to characterize CCL21's interaction with a related CCR7 peptide fragment (^{5}TDDYIGD^{11}), which occupied a surface on the α-helix of CCL21 with a K_d of 700 μM.[37] We titrated [U-^{15}N] CCL19 with increasing amounts of CCR7 5–11 peptide and observed substantial chemical shift perturbations for several CCL19 residues in the HSQC spectra (Fig. 4C). Nonlinear fitting of CCR7 5–11-induced shift perturbations yielded a K_d of 200 ± 100 μM (Fig. 4D). Based on this NMR analysis, the CCR7 5–11 peptide binds CCL19 with substantially lower affinity than the longer CCR7 2–30 peptide (12 μM) characterized previously by NMR.[1]

The CCR7 5–11 peptide perturbs residues throughout the CC19 sequence, but particularly on one side of the structure, with the majority clustering in the alpha helix (Fig. 4D & E). Many of these residues are basic amino acids or are near basic amino acids in primary structure (Fig. 4D). As CCL19 is a basic protein, with a theoretical pI of 9.84, while CCR7 5–11 is an acidic peptide with three aspartate residues, these chemical shift perturbation results suggest that electrostatic interactions play a dominant role in CCL19 binding of the receptor peptide. However, there are some potential hydrophobic contacts as well, as indicated by the perturbations of Ile21, Leu65, and Met72. Surrounded by nearby basic residues, some of these hydrophobic residues can potentially be involved in interacting with the tyrosine, or more than likely sulfotyrosine, in the full length, post-translationally modified CCR7 receptor.

Conclusion

We have solved the first X-ray crystal structure of the human chemokine CCL19, one of two ligands for the CCR7 receptor that guides T-cells and metastatic cancer cells into the draining lymph nodes. Our crystal structure illustrates unique structural features of CCL19, especially in the 30's loop, in comparison to the previously determined NMR structure. In our previous NMR analysis of the interaction of both CCL19 and CCL21 with the N-terminal domain of the CCR7 receptor (residues 1–30),[1, 37, 38] CCR7 binding caused chemical shift perturbations predominantly in the N-loop, third beta strand, and alpha helix for CCL19 and CCL21.[1, 37, 38] A shorter CCR7 peptide corresponding to residues 5–11 also bound weakly to the α-helix of CCL21.[37, 38] In comparison, CCR7 5–11 induced stronger shift perturbations across a larger region of the CCL19 surface but with the majority of the perturbations clustered in the α-helix, suggesting it as one of the main regions of contact. Interestingly, computational solvent mapping identified hot spots near the end of the α-helix in both CCL19 (Fig. 3A, CL02 and CL07) and CCL21 (Fig. 3B, CL03 and CL07). This region contains both positively charged and hydrophobic residues, making it suitable for interacting with the negatively charged aspartate residues and aromatic tyrosine side chain on the CCR7 peptide. These results provide valuable structural insights into the CCL19/CCL21/CCR7 signaling axis and can facilitate future development of small molecules targeting the chemokine-receptor interface, as demonstrated for CXCL12.[28, 40–43]

Acknowledgements

This work is supported by the National Institutes of Health (R01 GM097381 and S10 OD20000 to B.F.V.). Results shown in this report are derived from work performed at Argonne National Laboratory (ANL), Structural Biology Center (SBC) at the Advanced Photon Source (APS), under U.S. Department of Energy, Office of Biological and Environmental Research contract DE-AC02-06CH11357. This research used resources of the Advanced Photon Source; a U.S. Department of Energy (DOE) Office of Science User Facility operated for the DOE Office of Science by Argonne National Laboratory under Contract No. DE-AC02-06CH11357.

References

[1]. Veldkamp CT, Kiermaier E, Gabel-Eissens SJ, Gillitzer ML, Lippner DR, DiSilvio FA, Mueller CJ, Wantuch PL, Chaffee GR, Famiglietti MW, Zgoba DM, Bailey AA, Bah Y, Engebretson SJ, Graupner DR, Lackner ER, LaRosa VD, Medeiros T, Olson ML, Phillips AJ, Pyles H, Richard AM, Schoeller SJ, Touzeau B, Williams LG, Sixt M, and Peterson FC (2015) Solution Structure of CCL19 and Identification of Overlapping CCR7 and PSGL-1 Binding Sites, Biochemistry 54, 4163–4166. [PubMed: 26115234]

[2]. Mélik-Parsadaniantz S, and Rostène W (2008) Chemokines and neuromodulation, Journal of Neuroimmunology 198, 62–68. [PubMed: 18538863]

[3]. Forster R, Davalos-Misslitz AC, and Rot A (2008) CCR7 and its ligands: balancing immunity and tolerance, Nat Rev Immunol 8, 362–371. [PubMed: 18379575]

[4]. Harris NL, Jaffe ES, Stein H, Banks PM, Chan JK, Cleary ML, Delsol G, De Wolf-Peeters C, Falini B, Gatter KC, and et al. (1994) A revised European-American classification of lymphoid neoplasms: a proposal from the International Lymphoma Study Group, Blood 84, 1361–1392. [PubMed: 8068936]

[5]. Lopez-Giral S, Quintana NE, Cabrerizo M, Alfonso-Perez M, Sala-Valdes M, De Soria VG, Fernandez-Ranada JM, Fernandez-Ruiz E, and Munoz C (2004) Chemokine receptors that mediate B cell homing to secondary lymphoid tissues are highly expressed in B cell chronic lymphocytic leukemia and non-Hodgkin lymphomas with widespread nodular dissemination, J Leukoc Biol 76, 462–471. [PubMed: 15155773]

[6]. Love M, Sandberg JL, Ziarek JJ, Gerarden KP, Rode RR, Jensen DR, McCaslin DR, Peterson FC, and Veldkamp CT (2012) Solution structure of CCL21 and identification of a putative CCR7 binding site, Biochemistry 51, 733–735. [PubMed: 22221265]

[7]. Fernandez EJ, and Lolis E (2002) Structure, Function, and Inhibition of Chemokines, Annual Review of Pharmacology and Toxicology 42, 469–499.

[8]. Raju R, Gadakh S, Gopal P, George B, Advani J, Soman S, Prasad TSK, and Girijadevi R (2015) Differential ligand-signaling network of CCL19/CCL21-CCR7 system, Database (Oxford) 2015, bav106. [PubMed: 26504105]

[9]. Buonamici S, Trimarchi T, Ruocco MG, Reavie L, Cathelin S, Mar BG, Klinakis A, Lukyanov Y, Tseng JC, Sen F, Gehrie E, Li M, Newcomb E, Zavadil J, Meruelo D, Lipp M, Ibrahim S, Efstratiadis A, Zagzag D, Bromberg JS, Dustin ML, and Aifantis I (2009) CCR7 signalling as an essential regulator of CNS infiltration in T-cell leukaemia, Nature 459, 1000–1004. [PubMed: 19536265]

[10]. Weng AP, Ferrando AA, Lee W, Morris J. P. t., Silverman LB, Sanchez-Irizarry C, Blacklow SC, Look AT, and Aster JC (2004) Activating mutations of NOTCH1 in human T cell acute lymphoblastic leukemia, Science 306, 269–271. [PubMed: 15472075]

[11]. Cameron PU, Saleh S, Sallmann G, Solomon A, Wightman F, Evans VA, Boucher G, Haddad EK, Sekaly RP, Harman AN, Anderson JL, Jones KL, Mak J, Cunningham AL, Jaworowski A, and Lewin SR (2010) Establishment of HIV-1 latency in resting CD4+ T cells depends on chemokine-induced changes in the actin cytoskeleton, Proc Natl Acad Sci U S A 107, 16934–16939. [PubMed: 20837531]

[12]. Saleh S, Wightman F, Ramanayake S, Alexander M, Kumar N, Khoury G, Pereira C, Purcell D, Cameron PU, and Lewin SR (2011) Expression and reactivation of HIV in a chemokine induced model of HIV latency in primary resting CD4+ T cells, Retrovirology 8, 80. [PubMed: 21992606]

[13]. Finzi D, Hermankova M, Pierson T, Carruth LM, Buck C, Chaisson RE, Quinn TC, Chadwick K, Margolick J, Brookmeyer R, Gallant J, Markowitz M, Ho DD, Richman DD, and Siliciano RF (1997) Identification of a reservoir for HIV-1 in patients on highly active antiretroviral therapy, Science 278, 1295–1300. [PubMed: 9360927]

[14]. Crump MP, Gong JH, Loetscher P, Rajarathnam K, Amara A, Arenzana-Seisdedos F, Virelizier JL, Baggiolini M, Sykes BD, and Clark-Lewis I (1997) Solution structure and basis for functional activity of stromal cell-derived factor-1; dissociation of CXCR4 activation from binding and inhibition of HIV-1, Embo j 16, 6996–7007. [PubMed: 9384579]

[15]. Monteclaro FS, and Charo IF (1996) The amino-terminal extracellular domain of the MCP-1 receptor, but not the RANTES/MIP-1alpha receptor, confers chemokine selectivity. Evidence for a two-step mechanism for MCP-1 receptor activation, J Biol Chem 271, 19084–19092. [PubMed: 8702581]

[16]. Farzan M, Babcock GJ, Vasilieva N, Wright PL, Kiprilov E, Mirzabekov T, and Choe H (2002) The role of post-translational modifications of the CXCR4 amino terminus in stromal-derived factor 1 alpha association and HIV-1 entry, J Biol Chem 277, 29484–29489. [PubMed: 12034737]

[17]. Seibert C, and Sakmar TP (2008) Toward a framework for sulfoproteomics: Synthesis and characterization of sulfotyrosine-containing peptides, Biopolymers 90, 459–477. [PubMed: 17680702]

[18]. Huang C-C, Lam SN, Acharya P, Tang M, Xiang S-H, Hussan SS-U, Stanfield RL, Robinson J, Sodroski J, Wilson IA, Wyatt R, Bewley CA, and Kwong PD (2007) Structures of the CCR5 N terminus and of a tyrosine-sulfated antibody with HIV-1 gp120 and CD4, Science (New York, N.Y.) 317, 1930–1934.

[19]. Millard CJ, Ludeman JP, Canals M, Bridgford JL, Hinds MG, Clayton DJ, Christopoulos A, Payne RJ, and Stone MJ (2014) Structural basis of receptor sulfotyrosine recognition by a CC chemokine: the N-terminal region of CCR3 bound to CCL11/eotaxin-1, Structure 22, 1571–1581. [PubMed: 25450766]

[20]. Smith EW, Liu Y, Getschman AE, Peterson FC, Ziarek JJ, Li R, Volkman BF, and Chen Y (2014) Structural analysis of a novel small molecule ligand bound to the CXCL12 chemokine, J Med Chem 57, 9693–9699. [PubMed: 25356720]

[21]. Ziarek JJ, Liu Y, Smith E, Zhang G, Peterson FC, Chen J, Yu Y, Chen Y, Volkman BF, and Li R (2012) Fragment-based optimization of small molecule CXCL12 inhibitors for antagonizing the CXCL12/CXCR4 interaction, Curr Top Med Chem 12, 2727–2740. [PubMed: 23368099]

[22]. Battye TG, Kontogiannis L, Johnson O, Powell HR, and Leslie AG (2011) iMOSFLM: a new graphical interface for diffraction-image processing with MOSFLM, Acta Crystallogr D Biol Crystallogr 67, 271–281. [PubMed: 21460445]

[23]. (1994) The CCP4 suite: programs for protein crystallography, Acta Crystallogr D Biol Crystallogr 50, 760–763. [PubMed: 15299374]

[24]. Emsley P, and Cowtan K (2004) Coot: model-building tools for molecular graphics, Acta Crystallogr D Biol Crystallogr 60, 2126–2132. [PubMed: 15572765]

[25]. Joosten RP, Long F, Murshudov GN, and Perrakis A (2014) The PDB_REDO server for macromolecular structure model optimization, IUCrJ 1, 213–220.

[26]. Kozakov D, Grove LE, Hall DR, Bohnuud T, Mottarella SE, Luo L, Xia B, Beglov D, and Vajda S (2015) The FTMap family of web servers for determining and characterizing ligand-binding hot spots of proteins, Nat Protoc 10, 733–755. [PubMed: 25855957]

[27]. Veldkamp CT, Koplinski CA, Jensen DR, Peterson FC, Smits KM, Smith BL, Johnson SK, Lettieri C, Buchholz WG, Solheim JC, and Volkman BF (2016) Production of Recombinant Chemokines and Validation of Refolding, Methods Enzymol 570, 539–565. [PubMed: 26921961]

[28]. Smith EW, Lewandowski EM, Moussouras NA, Kroeck KG, Volkman BF, Veldkamp CT, and Chen Y (2016) Crystallographic Structure of Truncated CCL21 and the Putative Sulfotyrosine-Binding Site, Biochemistry 55, 5746–5753. [PubMed: 27617343]

[29]. Crump MP, Gong JH, Loetscher P, Rajarathnam K, Amara A, Arenzana-Seisdedos F, Virelizier JL, Baggiolini M, Sykes BD, and Clark-Lewis I (1997) Solution structure and basis for functional

activity of stromal cell- derived factor-1; dissociation of CXCR4 activation from binding and inhibition of HIV-1, Embo J 16, 6996–7007. [PubMed: 9384579]

[30]. Kleist AB, Getschman AE, Ziarek JJ, Nevins AM, Gauthier PA, Chevigne A, Szpakowska M, and Volkman BF (2016) New paradigms in chemokine receptor signal transduction: Moving beyond the two-site model, Biochem Pharmacol 114, 53–68. [PubMed: 27106080]

[31]. Gustavsson M, Dyer DP, Zhao C, and Handel TM (2019) Kinetics of CXCL12 binding to atypical chemokine receptor 3 reveal a role for the receptor N terminus in chemokine binding, Sci Signal 12, 3657.

[32]. Veldkamp CT, Seibert C, Peterson FC, Sakmar TP, and Volkman BF (2006) Recognition of a CXCR4 sulfotyrosine by the chemokine stromal cell-derived factor-1alpha (SDF-1alpha/CXCL12), J Mol Biol 359, 1400–1409. [PubMed: 16725153]

[33]. Veldkamp CT, Seibert C, Peterson FC, De la Cruz NB, Haugner JC 3rd, Basnet H, Sakmar TP, and Volkman BF (2008) Structural basis of CXCR4 sulfotyrosine recognition by the chemokine SDF-1/CXCL12, Sci Signal 1, ra4. [PubMed: 18799424]

[34]. Tan JH, Ludeman JP, Wedderburn J, Canals M, Hall P, Butler SJ, Taleski D, Christopoulos A, Hickey MJ, Payne RJ, and Stone MJ (2013) Tyrosine sulfation of chemokine receptor CCR2 enhances interactions with both monomeric and dimeric forms of the chemokine monocyte chemoattractant protein-1 (MCP-1), J Biol Chem 288, 10024–10034. [PubMed: 23408426]

[35]. Ludeman JP, and Stone MJ (2014) The structural role of receptor tyrosine sulfation in chemokine recognition, British journal of pharmacology 171, 1167–1179. [PubMed: 24116930]

[36]. Abayev M, Rodrigues J, Srivastava G, Arshava B, Jaremko L, Jaremko M, Naider F, Levitt M, and Anglister J (2018) The solution structure of monomeric CCL5 in complex with a doubly sulfated N-terminal segment of CCR5, FEBS J 285, 1988–2003. [PubMed: 29619777]

[37]. Phillips AJ, Taleski D, Koplinski CA, Getschman AE, Moussouras NA, Richard AM, Peterson FC, Dwinell MB, Volkman BF, Payne RJ, and Veldkamp CT (2017) CCR7 Sulfotyrosine Enhances CCL21 Binding, Int J Mol Sci 18, 1857.

[38]. Love M, Sandberg JL, Ziarek JJ, Gerarden KP, Rode RR, Jensen DR, McCaslin DR, Peterson FC, and Veldkamp CT (2012) Solution structure of CCL21 and identification of a putative CCR7 binding site, Biochemistry 51, 733–735. [PubMed: 22221265]

[39]. Fuchs JA, Brunner C, Schineis P, Hiss JA, and Schneider G (2019) Identification of Chemokine Ligands by Biochemical Fragmentation and Simulated Peptide Evolution, Angew Chem Int Ed Engl 58, 7138–7142. [PubMed: 30843649]

[40]. Veldkamp CT, Ziarek JJ, Peterson FC, Chen Y, and Volkman BF (2010) Targeting SDF-1/CXCL12 with a Ligand That Prevents Activation of CXCR4 through Structure-Based Drug Design, J Am Chem Soc 132, 7242–7243. [PubMed: 20459090]

[41]. Ziarek JJ, Liu Y, Smith E, Zhang G, Peterson FC, Chen J, Yu Y, Chen Y, Volkman BF, and Li R (2012) Fragment-Based Optimization of Small Molecule CXCL12 Inhibitors for Antagonizing the CXCL12/CXCR4 Interaction, Curr Top Med Chem 12, 2727–2740. [PubMed: 23368099]

[42]. Smith EW, Liu Y, Getschman AE, Peterson FC, Ziarek JJ, Li R, Volkman BF, and Chen Y (2014) Structural analysis of a novel small molecule ligand bound to the CXCL12 chemokine, J Med Chem 57, 9693–9699. [PubMed: 25356720]

[43]. Smith EW, Nevins AM, Qiao Z, Liu Y, Getschman AE, Vankayala SL, Kemp MT, Peterson FC, Li R, Volkman BF, and Chen Y (2016) Structure-Based Identification of Novel Ligands Targeting Multiple Sites within a Chemokine-G-Protein-Coupled-Receptor Interface, J Med Chem 59, 4342–4351. [PubMed: 27058821]

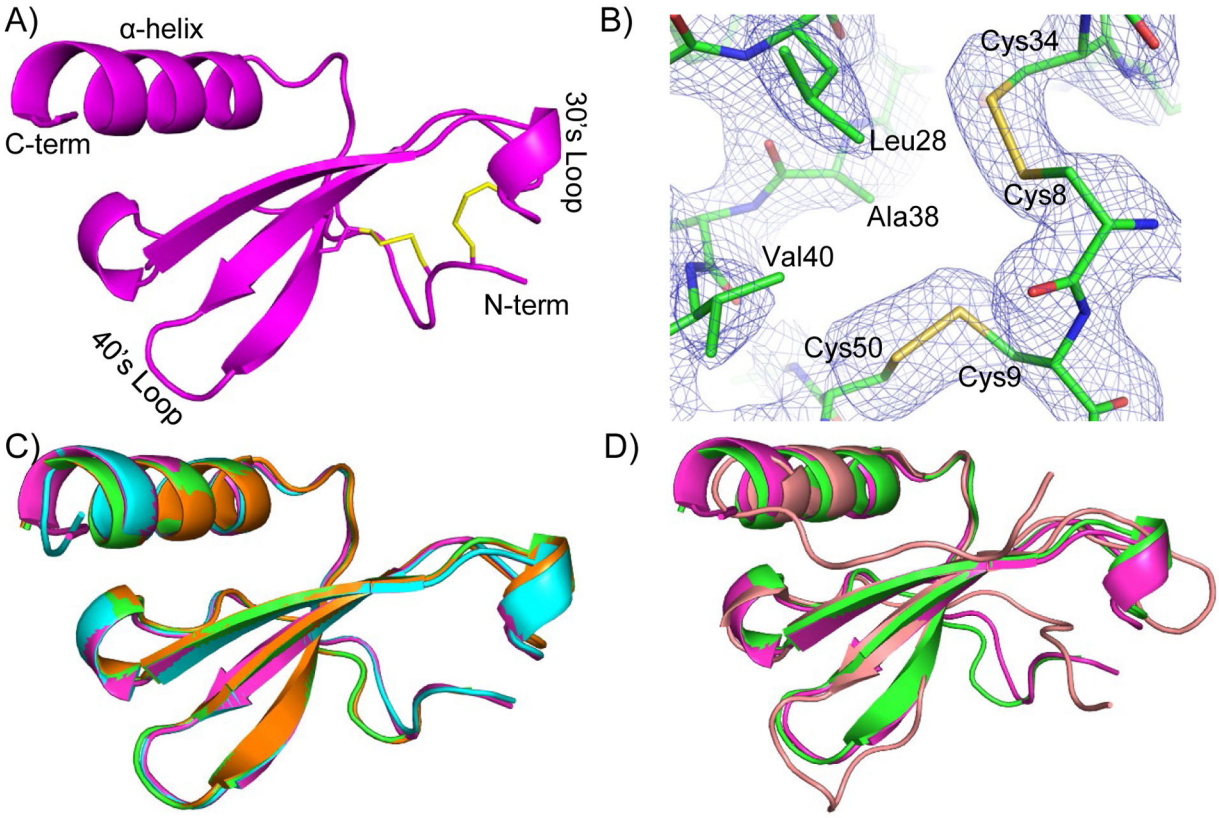

Figure 1. Crystal Structure of CCL19 7–70 Determined at 2.50 Å Resolution.

A) Monomer structure (Chain A) of CCL19. Disulfide bonds are shown as stick in yellow. Four monomers are present in each asymmetric unit. B) Representative electron density map showing the disulfide bonds for CCL19 (Chain B). $2F_O$-F_C density map (blue) is contoured at 1.0 σ. C) All four monomers in asymmetric unit superimposed. Chain A, B, C, and D are shown in magenta, green, cyan, and orange respectively. D) Chain A of the CCL21 crystal structure (PDB ID: 5EKI, salmon) superimposed onto Chain A (magenta) and Chain B (green) of CCL19 crystal structure (PDB ID: 7STA).

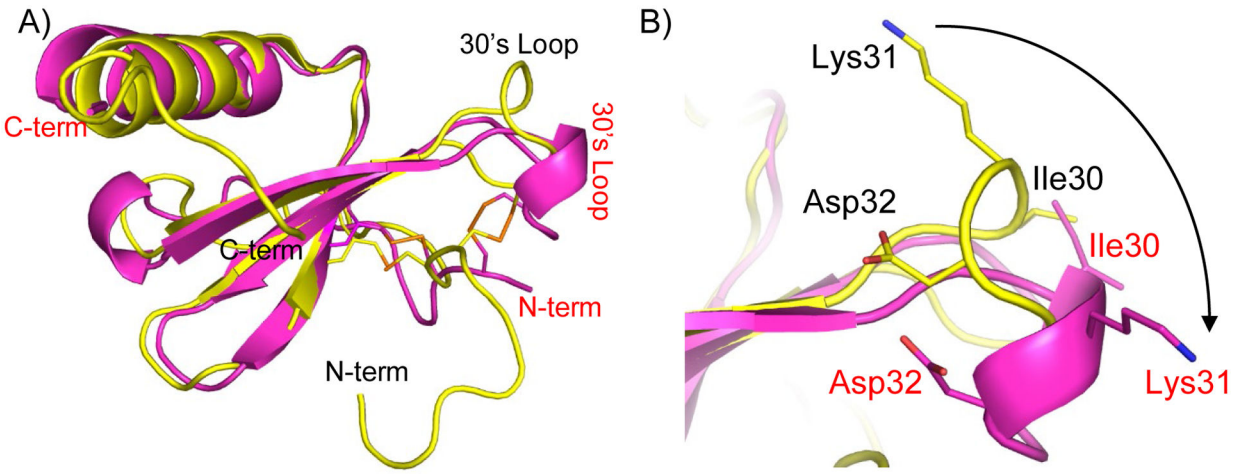

Figure 2. Comparison of CCL19 Crystal and NMR Structures.

A) Superimposition of the CCL19 NMR structure (PDB ID: 2MP1, yellow) onto Chain A of the CCL19 crystal structure (magenta). Disulfide bonds are shown as stick. B) Rotation of the 30's loop. In the crystal structure, the 30's loop is rotated downwards compared to its position in the NMR structure. This downwards position is not observed in any of the NMR ensemble poses. Labels and residue numbers are shown in red for the crystal structure, and black for the NMR structure.

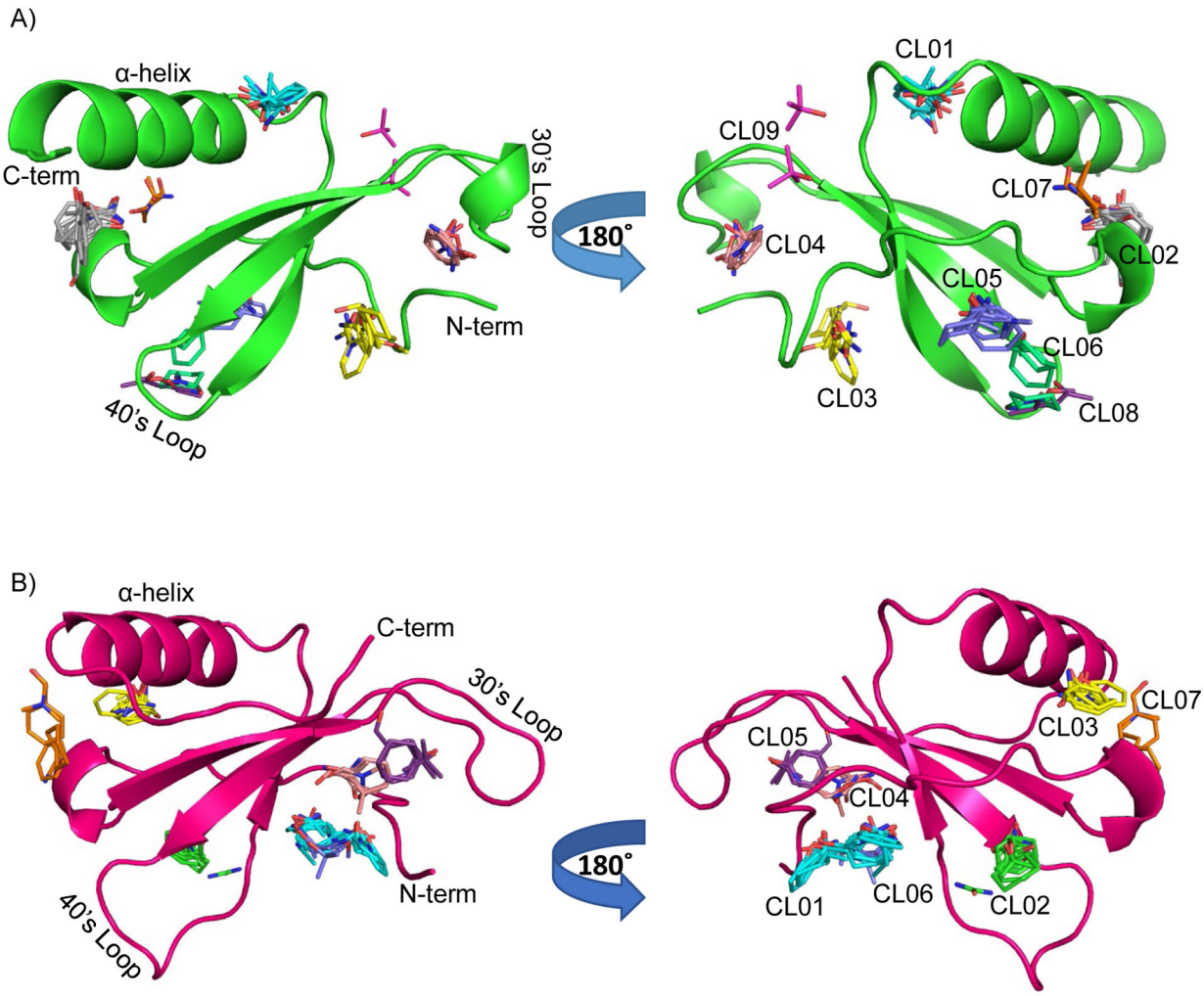

Figure 3. FTMap Analysis of CCL19 and CCL21 Crystal Structures.

A) FTMap analysis on Chain A of the CCL19 crystal structure shows nine probe clusters (CL01–09) in potential hot spots. CL01 (cyan) contains 20 probes; CL02 (silver) contains 17 probes; CL03 (yellow) contains 16 probes; CL04 (salmon) contains 13 probes; CL05 (light purple) contains 12 probes; CL06 (aqua) contains 6 probes; CL07 (orange) contains 6 probes; CL08 (dark purple) contains 4 probes; CL09 (magenta) contains 2 probes. CCL19 crystal structure is shown in green. B) FTMap analysis on Chain A of the CCL21 crystal structure (PDB ID: 5EKI) shows seven probe clusters (CL01–07) in potential hot spots. CL01 (cyan) contains 31 clusters; CL02 (green) contains 17 clusters; CL03 (yellow) contains 15 clusters; CL04 (salmon) contains 12 clusters; CL05 (dark purple) contains 8 clusters; CL06 (light purple) contains 7 clusters; CL07 (orange) contains 5 clusters. CCL21 crystal structure is shown in magenta.

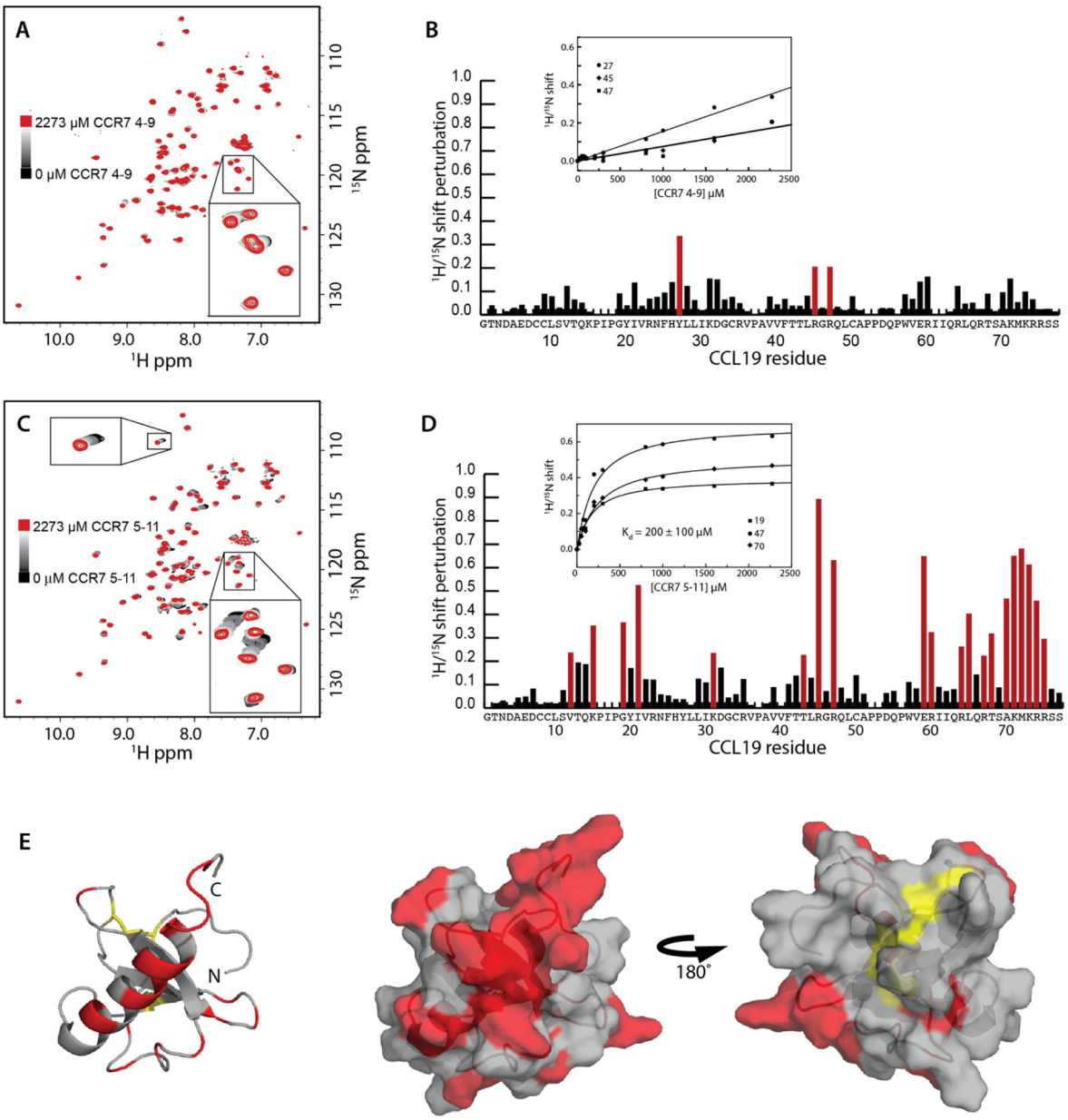

Figure 4. CCL19 Interactions with CCR7 5–11.

A) ^{15}N-^{1}H HSQC spectra of [U-^{15}N] CCL19 with increasing concentrations of CCR7 4–9. B) CCL19 chemical shift perturbations induced by the highest CCR7 4–9 concentration plotted versus CCL19 residue number with large perturbations indicated in red. (inset) CCL19 chemical shift perturbations plotted versus CCR7 4–9 concentration and nonlinear fitting indicating non-specific binding for residues 27, 45, and 47. C) ^{15}N-^{1}H HSQC spectra of [U-^{15}N] CCL19 with increasing concentrations of CCR7 5–11. D) CCL19 chemical shift perturbations induced by the highest CCR7 5–11 concentration plotted versus CCL19 residue number with large perturbations indicated in red. (inset) CCL19 chemical shift perturbations plotted versus CCR7 5–11 concentration and, representative, nonlinear fitting used for K_d determination for residues 19, 47, and 70. E) CCR7 5–11 induced chemical

shift perturbations (red) mapped onto the CCL19 solution structure (gray with disulfides highlighted in yellow).

Table 1.

X-ray Data Collection and Refinement Statistics

Data Collection	
Structure (PDB ID)	7STA
Space Group	$P2_1$
Cell Dimensions	
a, *b*, *c* (Å)	28.94
	148.18
	29.00
α, β, γ (°)	90.00
	90.07
	90.00
Resolution (Å)	49.39–2.50 (2.64–2.50)
No. Reflections	30636 (4601)
R_{merge} (%)	5.5 (29.1)
I / ó(I)	15.4 (5.0)
Completeness (%)	100.0 (100.0)
Redundancy	3.6 (3.7)
Refinement	
Resolution (Å)	37.07–2.50 (2.56–2.50)
R_{work}/R_{free} (%)	23.4/26.3
No. Heavy Atoms	
Protein	2046
Ligand/Ion	0
Water	1
***B*-Factors (Å²)**	
Protein	56.27
Ligand/Ion	0.00
Water	36.84
Ramanchandran Plot	
Most Favored Region (%)	96.1
Additionally Allowed (%)	3.4
Generously Allowed (%)	0.5

* Values in parentheses represent highest resolution shells